

# A Study of Enhancement in $\beta$ -phase and Dielectric Properties of $\text{Fe}_2\text{O}_3$ Reinforced in PVDF Nanocomposite Thin Films

Krishna Tewatia<sup>a\*</sup>, Anuradha Sharma<sup>a</sup>, Arun Kumar<sup>a</sup>, Kaushal Kumar<sup>a</sup>, Sohan Lal<sup>b</sup>, & Lakshmi Sowjanya Pali<sup>c</sup>

<sup>a</sup>J C Bose University of Science and Technology, YMCA, Faridabad 121 006, India

<sup>b</sup>National Institute of Technology, Kurukshetra 136 119, India

<sup>c</sup>VIT-AP University, Andhra Pradesh 522 237, India

Received: 10 May 2023; Accepted: 31 May 2023

Development of renewable energy resources can be an alternate source of fossil fuels and helpful in the reduction of pollution present in the environment. Having outstanding physical and chemical properties, polymer nanocomposites with enhanced piezoelectric properties are appropriate candidates for the development of renewable energy devices. Magnetite Iron oxide (II)  $\text{Fe}_2\text{O}_3$  is a narrow band gap metal oxide reinforced in Polyvinylidene Fluoride (PVDF) by solution casting method at 0.8, 1.6, 2.4 and 3.2wt.%. Dielectric and optical properties of nanocomposite thin films are analysed by impedance analyser and UV-visible spectroscopy. FTIR and RAMAN are used to analyse the enhancement in  $\beta$ -phase of nanocomposite thin films. Various parameters such as absorption coefficient, skin depth, optical density, electrical conductivity, and dielectric constant are calculated for the prepared samples. A significant increase in dielectric constant and  $\beta$ -phase is found after the reinforcement of  $\text{Fe}_2\text{O}_3$  nanoparticles. Dielectric constant and  $\beta$  phase are found to be maximum for higher concentrations of  $\text{Fe}_2\text{O}_3$ .  $\text{Fe}_2\text{O}_3$  embedded in PVDF nanocomposite thin films are suitable candidates for piezoelectric nanogenerators and pressure sensing devices.

**Keywords:** Nanocomposite Thin Films, Dielectric Properties, Metal Oxides, RAMAN Spectroscopy

## 1 Introduction

Energy harvesters are a good alternate source for the production of energy in recent time due to crises of energy and limited non-renewable sources. They collect ambient energy, which is present in the environment as vibrations, movements, light, heat, and magnetic energy. Due to the rise in wearable electronic gadgets, energy harvesting has recently been considered suitable for renewable energy devices<sup>1</sup>. In some situations, flexible self-powered gadgets can reduce their reliance on batteries by converting ambient energy into usable energy. Such portable gadgets can be made by piezoelectric materials which can generate energy by pressure or vibrations. There are many polymers like polyvinyl chloride (PVC), polyamide 11 (PA 11), PVDF and poly (vinylidene fluoride)-hexafluoro propylene (PVDF-HFP) having piezoelectric properties and can be used for energy harvesting. Being a thermoplastic semicrystalline polymer, polyvinylidene fluoride (PVDF) is an appropriate candidate to use in piezoelectric devices. PVDF is a light weight, low

cost, flexible and low-density polymer. PVDF has five phases with different chain arrangements  $\alpha$ ,  $\beta$ ,  $\gamma$ ,  $\delta$  and  $\epsilon$ <sup>2,3</sup>.  $\beta$  and  $\gamma$  phases are responsible for the piezoelectric properties of PVDF. To achieve the electroactive  $\beta$  and  $\gamma$  phases in PVDF, several attempts have been made, including mechanical stretching, melt quenching, applying electric field, electro spinning, and many others<sup>4,5,6</sup>.  $\beta$ -phase has largest spontaneous polarization, specific chain arrangement indicating the highest ferroelectric, piezoelectric and pyroelectric behaviour. Various methods such as nucleating filler, solvent casting, phase transition and co-polymerisation can be used for the synthesis of nanocomposite films. Addition of nanoparticles to PVDF matrix can increase the  $\beta$ -phase and dielectric permittivity for the possible use in piezoelectric energy storage devices. The  $\alpha$ -phase having highest thermodynamic stability and paraelectricity, is frequently employed for painting and insulating due to its poor heat conductivity, low chemical and thermal resistance. The  $\delta$ -phase exhibits ferroelectric behaviour and polar phase. The  $\alpha$ -phase can be transformed into the polar  $\beta$  and  $\gamma$ -phase by many methods. They are extensively used in sensors,

\*Corresponding author (E-mail: kuntalkrishna111@gmail.com)

batteries, actuators, and energy collecting systems<sup>7</sup>. Also, the electroactive  $\beta$ -phase of polymer can be improved by addition of ferrite nanoparticles, hydrated ionic salts  $\text{TiO}_2$ ,  $\text{BaTiO}_3$ , and clays<sup>8,9,10</sup>. Mechanical properties can be improved by enhancement of interfacial stability between polymer and nanoparticles. Ionic conductivity also can be enhanced by reducing the crystallinity of the host polymer and interaction between the polar groups of the metal and the electrolyte ionic species.

To enhance the optical, dielectric, and electrical characteristics of polymer nanocomposites, iron oxide may be a good candidate for polymer nanocomposites. Iron oxide occur in a variety of forms with various stoichiometry and crystalline phases hematite (Fe), wurzite (FeO), magnetite ( $\text{Fe}_3\text{O}_4$ ), maghemite ( $-\text{Fe}_2\text{O}_3$ ), and ( $-\text{Fe}_2\text{O}_3$ ). Metal oxide  $\text{Fe}_2\text{O}_3$  is a thermodynamically stable semiconductor material. It is inexpensive, stable at high temperatures, and naturally non-toxic<sup>11</sup>. Various works Al/ $\text{Fe}_2\text{O}_3$ /PVDF composites<sup>12</sup>, PVDF membrane with  $\text{Fe}_2\text{O}_3$  particles and multi wall carbon nano tubes (MWCNT)<sup>13</sup>,  $\alpha$ - $\text{Fe}_2\text{O}_3$ /PVDF-HFP<sup>14</sup>, Chi@ $\text{Fe}_2\text{O}_3$ -PVDF-based filtration<sup>15</sup>, transition metal oxide/PVDF composites<sup>16</sup>,  $\alpha$ - $\text{Fe}_2\text{O}_3$ @PVDF electrode<sup>17</sup>, maghemite/PVDF nanogenerators are reported in literature. Martins *et al.* found that PVDF/ferrite nanocomposites, 90% of the  $\beta$ -phase was achieved by melt processing along with addition 5 wt% of  $\text{CoFe}_2\text{O}_4$  and 50 wt% of  $\text{NiFe}_2\text{O}_4$ <sup>18</sup>. Prabhakaran *et al.* noted that 0.14 wt% of ferrite concentration causes the maximum polarization and magnetization values. This optimum composition reveals good ferroelectric and piezoelectric response<sup>19</sup>.

Goncalves *et al.* reported that the incorporation of 15nm  $\text{Fe}_2\text{O}_3$  nanoparticles enhanced the nucleation and the  $\beta$ -phase<sup>20</sup>. Ouyang *et al.* revealed that addition of magnetite nanoparticles increases the storage modulus in nanocomposites. They also found that the incorporation of 2wt% iron oxide in polymer enhanced the piezoelectric properties around five times with the applied strength of the electrical field at  $35\text{MV}/\text{m}^2$ . Only limited number of authors has been worked on

the optical and dielectric properties of  $\text{Fe}_2\text{O}_3$ /PVDF nanocomposite thin films.  $\text{Fe}_2\text{O}_3$  can be used for improving optical characteristics because of its high refractive index and band gap (2.2 eV) in the visible spectrum. It has been considered a worthy candidate for several optical applications. The incorporation of  $\text{Fe}_2\text{O}_3$  nanoparticles in PVDF causes the charge distribution and transportation of the dielectric components, ultimately enhancing the conductivity of the host polymer. Furthermore, changes in the piezoelectric, magnetic and dielectric response of the nanocomposites are found to be influenced by the concentration of iron-oxide nanoparticles. Here, we have focused on the reinforcement of  $\text{Fe}_2\text{O}_3$  in PVDF by simple solvent casting method at different wt.%. Absorption coefficient ( $\alpha$ ), skin depth ( $\delta$ ), optical density, dielectric constant, electrical and optical conductivity are calculated by UV visible data. FTIR and RAMAN spectroscopy are used to find the change in phase of nanocomposite thin films.  $\beta$ -phase and dielectric properties are improved after addition of  $\text{Fe}_2\text{O}_3$  nanoparticles.

## 2 Materials and Methods

The synthesis route for the preparation of  $\text{Fe}_2\text{O}_3$  reinforced PVDF nanocomposite is schematically shown in Fig. 1. Iron rust is collected from waste material and washed several times with deionised water. Dried iron rust is mechanically ground with mortar pastel for six hours. The collected iron oxide particles are reinforced in prepared PVDF solution with DMF at 0.8, 1.6, 2.4 and 3.2wt.%.The solution is stirred for 10 hours and probe sonicated for two hours. Final solution is poured on a glass slide cleaned by acetone and ethanol. The poured solution is dried in hot air oven at  $110^\circ\text{C}$  for three hours. The dried nanocomposite thin films are peeled off with help of doctor blade. The free standing thin films are shown in Fig. 1.

Shimadzu UV-Visible (UV-Vis) Spectroscopy records absorbance and reflectance data for the purpose of studying various optical and electrical properties. PerkinElmer FTIR is used to study the

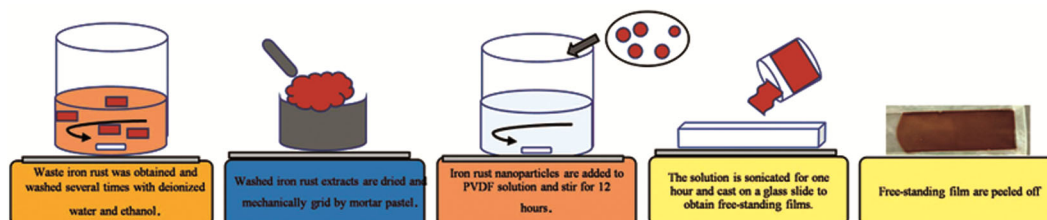


Fig. 1 — Schematic diagram of synthesis of  $\text{Fe}_2\text{O}_3$ /PVDF nanocomposite thin films.

change in phase of nanocomposite thin films. A two probe LCR meter (Hioki 3532-50 LCR Hitester) at room temperature is used to measure the capacitance value to calculate the dielectric constant and dissipation factor.

### 3 Results and Discussion

#### 3.1 UV-visible spectroscopy

Figure 2 shows absorption spectra and Fig. 3 shows the band gap of Fe<sub>2</sub>O<sub>3</sub> nanoparticles. The direct band gap of particles is calculated by using equation (1) by Tauc's plot<sup>22,23</sup>. The direct band of Fe<sub>2</sub>O<sub>3</sub> nanoparticles is found to be 2.08eV. Figure 4(a) illustrates how the absorption coefficient ( $\alpha$ ) of nanocomposite thin films varies with wavelength ( $\lambda$ ).

$\alpha$  is maximum at the highest concentrations at shorter wavelengths and progressively diminishes as wavelength rises. Due to the greater absorption of Fe<sub>2</sub>O<sub>3</sub> nanoparticles,  $\alpha$  increases as Fe<sub>2</sub>O<sub>3</sub>

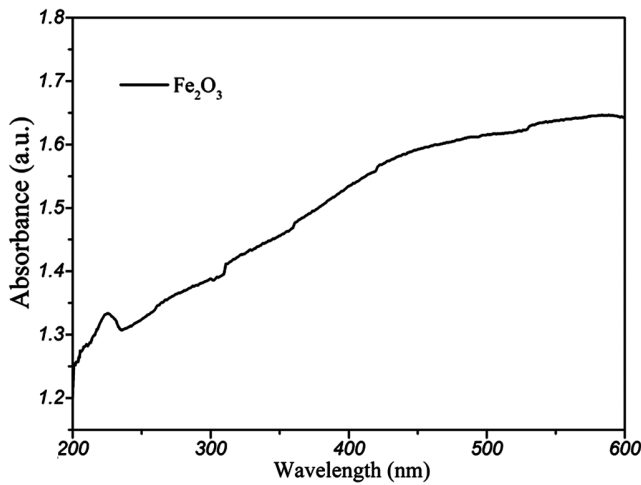


Fig. 2 — Plot of absorption spectra of Fe<sub>2</sub>O<sub>3</sub> particles.

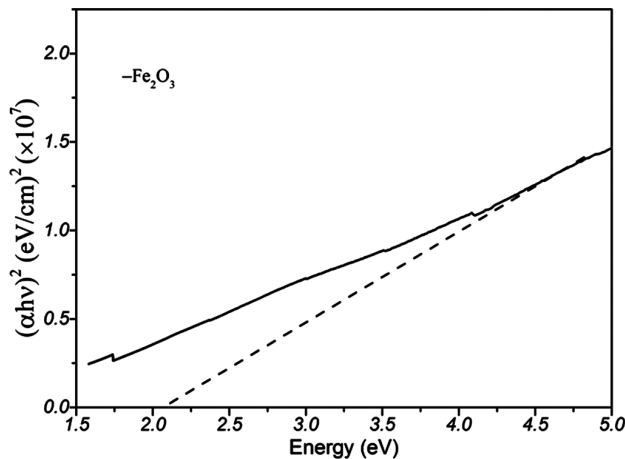


Fig. 3 — Plot of band gap of Fe<sub>2</sub>O<sub>3</sub> particles.

concentrations rises. Equation (2) may be used to compute  $\alpha$ , which was found to be strongly influenced by the film thickness and absorption. Thin films, in comparison to bulk materials<sup>8</sup>, exhibit greater improvement in  $\alpha$ . At larger concentrations, the maximum value of  $\alpha$  is obtained 724 around 320nm.

$$(\alpha hv) = B(hv - E_g)^n \quad \dots (1)$$

$$\alpha = \frac{\ln(I_0/I)}{t} = -\frac{\ln(T)}{t} = 2.303 \left(\frac{A}{t}\right) \quad \dots (2)$$

The nanocomposite film's transmittance reduces when the amount of Fe<sub>2</sub>O<sub>3</sub> is increased, as seen in Fig. 4(b). In the visible range, transmittance is constant, but it decreases in the UV range and rises in the near IR region. The decreased transmittance could be due to the Rayleigh scattering of light by Fe<sub>2</sub>O<sub>3</sub> nanoparticles. Other factors that may influence the transmittance spectra of nanocomposite thin films include the film's roughness, particle dispersion, refractive index, and interactions between polymers and Fe<sub>2</sub>O<sub>3</sub>.

$$\delta = \frac{1}{\alpha} \quad \dots (3)$$

$$D_{opt} = \alpha t \quad \dots (4)$$

Skin depth and optical density varies as shown in Fig. 4(c) and (d). The measurement of the wave penetration into the film is measured by a physical phenomenon known as skin depth of a material. A reduction in skin depth reveals the penetration of EM wave absorption inside the nanocomposite thin films<sup>25</sup>.

$$\sigma_{opt} = \frac{\alpha \eta c}{4\pi} \text{ and } \sigma_e = \frac{2\pi}{\eta c} \quad \dots (5)$$

Additionally, significant connections between skin depth, UV ray energy, and Fe<sub>2</sub>O<sub>3</sub> content was observed. As the amount of Fe<sub>2</sub>O<sub>3</sub> rises in the current investigation, the skin depth decreases and is reported as 0.00143 at 3.2eV for 4wt%. In low energy areas, skin depth is maximum, and diminished in high energy region. Optical density has smaller values in low energy regions but increase in higher energy regions. The optical density depends on the film's thickness and absorption coefficient. The optical density was found to be 2.68 at 1.85eV for 4wt.% of Fe<sub>2</sub>O<sub>3</sub> particles. Optical and electrical conductivity can be calculated by equation (5) as shown Fig. 4(e) and (f). It is observed that optical conductivity has a direct relation with the refractive index and the absorption coefficient. Optical conductivity gives

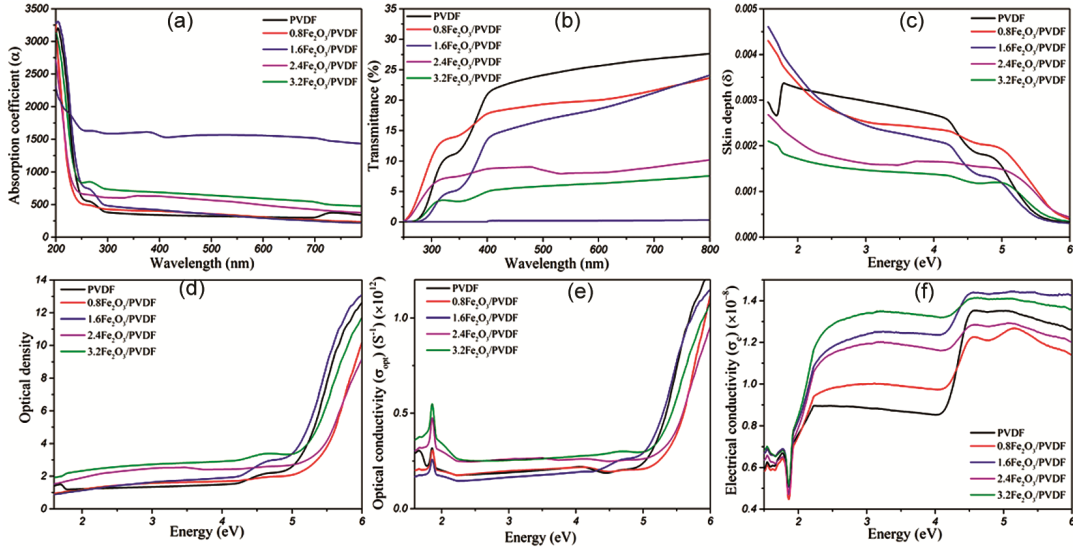


Fig. 4 — Plot of (a) absorption coefficient ( $\alpha$ ), (b) transmittance spectra, (c) skin depth ( $\delta$ ), (d) optical density, (e) optical conductivity and (f) electrical conductivity of  $\text{Fe}_2\text{O}_3/\text{PVDF}$  nanocomposite thin films.

Table 1 — Variation of Absorption coefficient, optical density, skin depth,  $\beta$  fraction, optical and electrical conductivity with different wt.% of  $\text{Fe}_2\text{O}_3$ .

Sample	Absorption coefficient ( $\alpha$ )	Optical density	Skin depth	Optical conductivity ( $\times 10^{12}$ )	Electrical conductivity ( $\times 10^{-8}$ )	$\beta$ fraction	Dielectric constant
PVDF	371	1.32	0.00288	0.3127	0.8826	71.37694	14.73
0.8wt.% $\text{Fe}_2\text{O}_3/\text{PVDF}$	421	1.59	0.00247	0.3104	1.000	73.04388	15.13
1.6wt.% $\text{Fe}_2\text{O}_3/\text{PVDF}$	469	1.61	0.00232	0.2728	1.24	79.70738	15.01
2.4wt.% $\text{Fe}_2\text{O}_3/\text{PVDF}$	604	2.45	0.00159	0.4724	1.195	76.64808	15.18
3.2wt.% $\text{Fe}_2\text{O}_3/\text{PVDF}$	724	2.68	0.00143	0.5484	1.34	80.29197	15.38

information on the electrical behaviour of the material and the redistribution of charge during interactions with light. With increasing  $\text{Fe}_2\text{O}_3$  content, optical conductivity increases until it reaches a maximum of  $5.48 \times 10^{11}$  at 4wt.%. In the low energy region, optical conductivity is highest at  $\sim 1.85$  eV; as energy rises it starts to decline and further increases in higher energy regions. The existence of impurities can lead to inter-band transition, and certain peaks in optical conductivity indicate that electromagnetic waves have penetrated deeply.  $\text{Fe}_2\text{O}_3$  nanoparticle reinforcement results in an improvement in conductivity because of more charge transfer excitations occurring inside the nanocomposite films. In addition to having an effect on absorption coefficient, surface shape also affects the variation in conductivity. Electrical conductivity and refractive index have an inverse relationship<sup>26</sup>. It decreases in the low energy region and rises in the high energy region. The  $\text{Fe}_2\text{O}_3$  nanoparticles act as centres for the scattering and trapping of the charged carriers. Because more charge carriers are being trapped when the concentration of nanofillers increases, electrical

conductivity falls. Higher electrical conductivity is caused by improved interfacial contact between the structure of the nanocomposite and the nanofillers, which results in increased charge transfer.

### 3.2 FTIR and RAMAN analysis

Figure 5 shows the FTIR spectra of nanocomposite thin films of doped and undoped PVDF. The nanocomposite films show distinctive absorption bands at 840, 1175, and 1279 $\text{cm}^{-1}$  referred to as the piezoelectric crystalline phase. The  $\beta$ -phase content of the PVDF polymer was improved by addition of  $\text{Fe}_2\text{O}_3$  nanoparticles. The PVDF crystallizes most strongly in the  $\beta$  phase at 1175 $\text{cm}^{-1}$  when  $\text{Fe}_2\text{O}_3$  is added, although the  $\gamma$ -phase crystallization at 1234  $\text{cm}^{-1}$  also increases with the same dopant ratio<sup>27</sup>. Both heterogeneous nucleation and isothermal crystallization of PVDF nanocomposite are enhanced by the presence of  $\text{Fe}_2\text{O}_3$  nanoparticles. By limiting the mobility of polymer chains, it affects the crystallization as filler concentration rises. For  $\alpha$ ,  $\beta$ , and  $\gamma$  phases, specific peaks can be utilized to determine the relative amount

of each phase for both identification and quantification. In our case 440, 480, 837, 875, 1170 and 1400 $\text{cm}^{-1}$  peaks occur for  $\beta$ -phase formation. Peaks at 510, 610 and 764 $\text{cm}^{-1}$  represent the  $\alpha$  phase and 1232 $\text{cm}^{-1}$  for  $\gamma$ -phase.  $\beta$ -phase was noted enhanced and more stable.  $\beta$ -phase improve up to 80% for 3.2wt.%  $\text{Fe}_2\text{O}_3$ . Infrared absorption bands at 764 and 837 $\text{cm}^{-1}$ , which are indicative of the  $\alpha$  and  $\beta$  phases, were used to calculate the amount of  $\alpha$  and  $\beta$  phase materials contained in each sample respectively. Equation (6) may be used to compute the  $\beta$  phase fraction,  $F(\beta)$ .

$$F(\beta) = A_{\beta} / \left( \left( \frac{K_{\beta}}{K_{\alpha}} \right) A_{\alpha} + A_{\beta} \right) \quad \dots (6)$$

Figure 6 shows the RAMAN spectra of  $\text{Fe}_2\text{O}_3/\text{PVDF}$  thin films. Raman spectra indicate a formation of  $\beta$ -phase at 512, 837 and 1074 $\text{cm}^{-1}$  peaks.

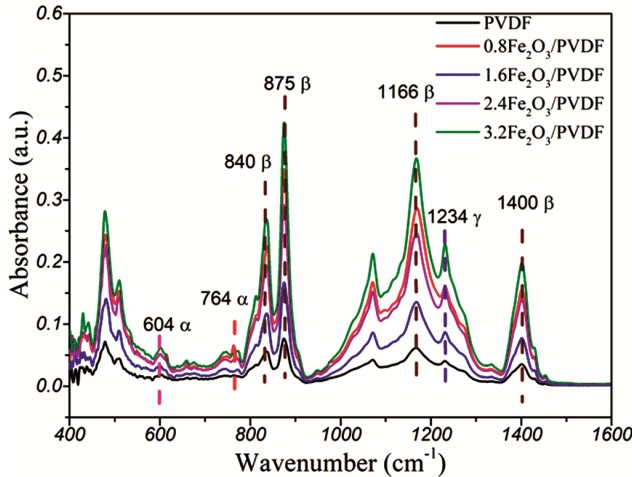


Fig. 5 — FTIR spectra of  $\text{Fe}_2\text{O}_3/\text{PVDF}$  nanocomposite thin films.

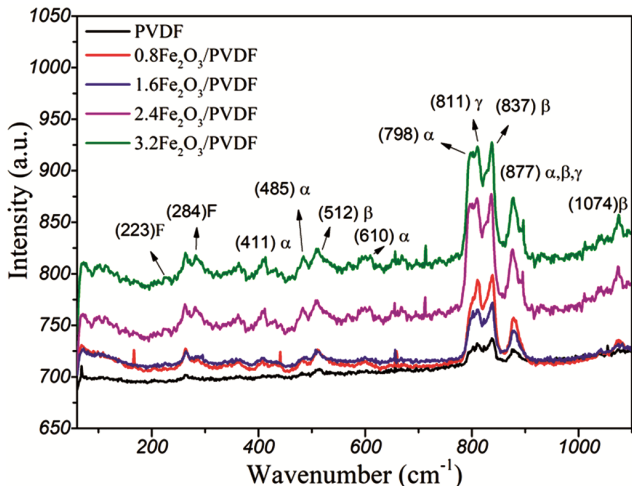


Fig. 6 — RAMAN spectra of  $\text{Fe}_2\text{O}_3/\text{PVDF}$  nanocomposite thin films.

Peaks at 410, 485, 610 and 798 $\text{cm}^{-1}$  occur due to presence of  $\alpha$ -phase. In addition, a common peak at 877 $\text{cm}^{-1}$  appear for  $\alpha$ ,  $\beta$  and  $\gamma$  phases. Raman scan shows that  $\beta$ -phase are stabilized in films. Peaks induced by the metal oxide  $\text{Fe}_2\text{O}_3$  are present at 223 and 284 $\text{cm}^{-1}$ . However, the Raman image intensity increased along with the amount of  $\text{Fe}_2\text{O}_3$ , and the impact of crystallinity was noted. Additionally, the FTIR pictures and Raman images are in perfect agreement.

### 3.3 Dielectric analysis

Figure 7 illustrates the dielectric behaviour of nanocomposites as a function of frequency. At a concentration of 3.2wt% of nanoparticles, the dielectric constant for  $\text{Fe}_2\text{O}_3/\text{PVDF}$  thin films is 15.38. This increase in the dielectric constant value of the nanocomposite is the result of interfacial polarization with charge accumulation and short-range dipole-dipole interactions at the  $\text{Fe}_2\text{O}_3/\text{PVDF}$  film interface with the electrical field. The dielectric constant is impacted by the frequency-dependent decrease in aligned dipole number. The dipoles also lag the applied electric field at higher frequencies. The augmentation of the dielectric constant value is influenced by interfacial area per unit volume of the nanoparticle<sup>28</sup>. Greater average polarization and interparticle interaction result from lower interparticle distance per unit volume at higher interfacial areas. Additionally, the inclusion of  $\text{Fe}_2\text{O}_3$  nanoparticles, which also help to increase the dielectric constant, enhances the beta phase of the PVDF. Figure 8 shows the plot of dissipation factor with frequency. Dissipation factor first decrease and increase further at higher frequencies.

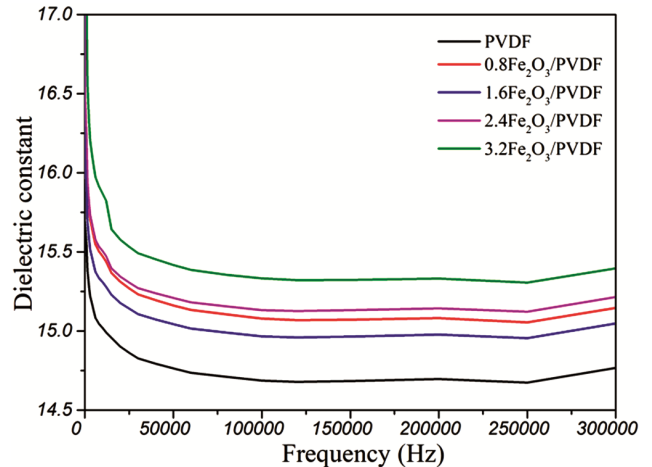


Fig. 7 — Plot of dielectric constant of  $\text{Fe}_2\text{O}_3/\text{PVDF}$  nanocomposite thin films.

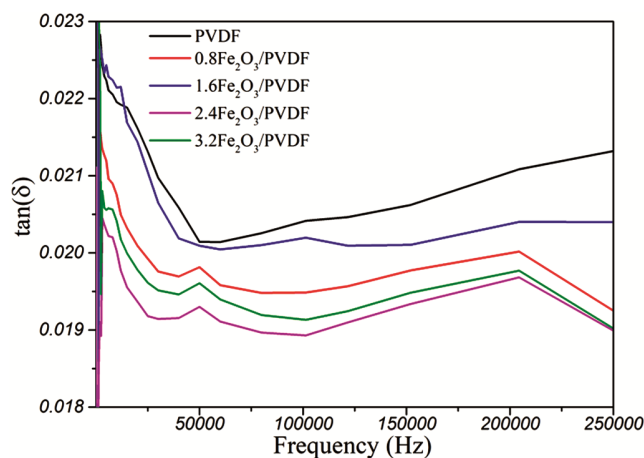


Fig. 8 — Plot of dissipation factor of  $\text{Fe}_2\text{O}_3/\text{PVDF}$  nanocomposite thin films.

#### 4 Conclusions

This article reports a simple and cost-effective method for preparation of  $\text{Fe}_2\text{O}_3/\text{PVDF}$  nanocomposite thin films. UV visible, FTIR, RAMAN and dielectric measurement are used to analyze the effect of  $\text{Fe}_2\text{O}_3$  nanoparticles on optical, piezoelectric, and dielectric properties. The direct bandgap of  $\text{Fe}_2\text{O}_3$  is 2.1 eV as obtained from UV-Vis spectroscopy and enhancement in absorption coefficient, optical density, optical and electrical conductivity. Skin depth decreases and is found to have application in EMI shielding. FTIR and RAMAN spectra confirm the enhancement in  $\beta$ -phase responsible for piezoelectric properties.  $\beta$ -phase improves up to 80% for 3.2 wt.% filler. Dielectric constant was noted to be improved after reinforcement of  $\text{Fe}_2\text{O}_3$  and increase with increases in concentration of filler. Dielectric constant was found to 15.38 at higher concentration.  $\text{Fe}_2\text{O}_3/\text{PVDF}$  nanocomposite thin films have considerable applications in piezoelectric and energy storage devices.

#### References

- 1 Fatma B, Bhunia R, Gupta A, Verma A, Verma V, Garga A, *ACS Sustainable Chemistry & Engineering*, 7 (2019) 14856.
- 2 Salimi A & Yousefi A, *J Polym Sci Part B*, 42 (2004) 3487.
- 3 Pramod K P, Mohamed A, Yee Phang I & Liu T, *Polym Int*, 54 (2005) 226.
- 4 Scheinbeim J I, Newman B A & Sen A, *Macromolecules*, 19 (1986) 1454.
- 5 Wang J, Li H, Liu J, Duan Y, Jiang S, & Yan S, *J Am Chem Soc*, 125 (2003) 1496.
- 6 Pickford T, Gu X, Heeley E L & Wan C, *Cryst Eng Comm*, 21 (2019) 5418.
- 7 Pan Z, Wang M, Chen J, Shen B, Liu J, & Zhai J, *Nanoscale*, 10 (2018) 16621.
- 8 Mendes S F, Costa C M, Caparros C, Sencadas V & Lanceros-Me'ndez S, *J Mater Sci*, 47 (2012) 1378.
- 9 Patro T U, Mhalgi M V, Khakhar D V & Misra A, *Polymer*, 49 (2008) 3486.
- 10 Martins P, Costa C M & Lanceros-Mendez S, *Appl Phys A*, 103 (2011) 233.
- 11 Zotti G, Schiavon G, Zecchin S & Casellato U, *J Electrochem Soc*, 385 (1998).
- 12 Lee J H, Kim S, Hun Lee J, Jin Kim S, Soo Park J & Hak Kim J, *Macromol Res*, 24 (2016) 909.
- 13 Lovinger A J, *Science*, 220 (1983) 1115.
- 14 Bhatt P, Upadhyay A, Bhatt R, Yusuf S M, *AIP Conference Proceedings*, 2115 (2019) 030567.
- 15 Ohgo K, Zhao C, Kobayashi M & Asakura T, *Polymer*, 44 (2003) 841.
- 16 Chai M, Tong W, Wang Z, Chen Z, & An Y, Zhang Y, *J Hazard Mater*, 430 (2022) 128446.
- 17 Park J E, Shin J H, Oh W, Choi S J, Kim J, Kim C, & Jeon J, *Toxics*, 10 (2022) 98.
- 18 Xu L, Sitinamaluwa H, Li H, Qiu J, Wang Y, Yan C, Li H, Yuan S, & Zhang S, *J Mater Chem A*, 5 (2017) 2102.
- 19 Prabhakaran T & Hemalatha J, *Mater Chem Phys*, 137 (2013) 781.
- 20 Goncalves R, Martins P M, Caparros C P & Martins, M, *J Non Cryst Solid*, 361 (2013) 93.
- 21 Ouyang Z W, Chen E C & Wu T M, *Materials*, 8 (2015) 4553.
- 22 Qayoom M, Bhat R, Shah K A, Pandit K H, Firdous A, & Dar G A, *J Electron Mater*, 49 (2020) 2.
- 23 Al-Ramadin Y, *Opt Mater*, 14 (2000) 287.
- 24 Benchaabane A, Hajlaoui M E, Hnainia N, Tabbakh A A, Zeinert A, & Bouchriha H, *Opt Mater*, 102 (2020) 109829.
- 25 Pasha A & Ab d El -Rehim A F, *Ceram Int*, (2022) 1.
- 26 Yousaf M, Khan M J I, Kanwal Z, Ramay S M, Shaikh H, & Salim M, *Polym Bull*, 79 (2022) 9975.
- 27 Ongun M Z, Paral L, Oguzlar S & Pechousek J, *J Mater Sci Mater Electron*, 31 (2020) 19146.
- 28 AlAhzm A M, Alejli M O, Ponnamma D, Elgawady Y & Maadeed M A A A, *J Mater Sci Mater Electron*, 32 (2021) 14610.